

## THE SIZE EVOLUTION OF HIGH REDSHIFT GALAXIES<sup>1</sup>

HENRY C. FERGUSON<sup>2,3</sup>, MARK DICKINSON<sup>2,3</sup>, MAURO GIAVALISCO<sup>2,11</sup>, CLAUDIA KRETCHMER<sup>3</sup>, SWARA RAVINDRANATH<sup>2</sup>,  
 RAFAL IDZI<sup>3</sup>, EDWARD TAYLOR<sup>4</sup>, CHRISTOPHER J. CONSELICE<sup>5</sup>, S. MICHAEL FALL<sup>2</sup>, JONATHAN P. GARDNER<sup>6</sup>, MARIO  
 LIVIO<sup>2</sup>, PIERO MADAU<sup>7</sup>, LEONIDAS A. MOUSTAKAS<sup>2</sup>, CASEY M. PAPOVICH<sup>8</sup>, RACHEL S. SOMERVILLE<sup>2</sup>, HYRON SPINRAD<sup>9</sup>,  
 DANIEL STERN<sup>10,11</sup>

*Draft version October 26, 2018*

### ABSTRACT

Hubble Space Telescope images of high-redshift galaxies selected via color and photometric redshifts are used to examine the size and axial-ratio distribution of galaxies as a function of redshift at lookback times  $t > 8$  Gyr. These parameters are measured at rest-frame UV wavelengths ( $1200 < \lambda < 2000 \text{ \AA}$ ) on images with a rest-frame resolution of less than 0.8 kpc. Galaxy radii are found to scale with redshift approximately as Hubble parameter  $H^{-1}(z)$ . This is in accord with the theoretical expectation that the typical sizes of the luminous parts of galaxies should track the expected evolution in the virial radius of dark-matter halos. The mean ratio of semi-major to semi-minor axis for a bright well-resolved sample of galaxies at  $z \sim 4$  is  $b/a = 0.65$ , suggesting that these Lyman break galaxies are not drawn from a spheroidal population. However the median concentration index of this sample is  $C = 3.5$ , which is closer to the typical concentration indices,  $C \sim 4$ , of nearby elliptical galaxies than to the values,  $C < 2$  for local disk galaxies of type Sb and later.

*Subject headings:* Galaxies: evolution — Galaxies: high-redshifts — Galaxies: structure — Cosmology: observations

### 1. INTRODUCTION

An important goal of cosmology is to understand how galaxies evolve toward their current sizes and shapes. The basic framework of galaxy formation within the hierarchical Cold-Dark-Matter (CDM) cosmology was set out by White & Rees (1978), and has been refined by numerous N-body and semi-analytical studies (Cole et al. 1994; Kauffmann et al. 1993; Somerville & Primack 1999; White & Frenk 1991). The formation of galactic disks within dark-matter halos was studied by Fall & Efstathiou (1980). In this model, dark halos acquire their angular momenta via tidal torques, the angular momentum per unit mass of the baryons and the dark matter are initially the same, and angular momentum is conserved as the baryons collapse and cool to form a disk. With these simplifying assumptions the baryons typically collapse by factors

of  $\sim 10$  and the resulting disks have rotation curves, surface-density profiles, and scale radii similar to those observed. Further analytical studies have calculated the distribution function of disk-galaxy sizes and the disk-galaxy size-redshift relation (Dalcanton et al. 1997; Mo et al. 1998). Meanwhile cosmological N-body + hydrodynamical simulations have formed disks that appear similar to spiral galaxies, but that tend to be too small to match present-day galaxies (Navarro & Steinmetz 1997; but see Eke et al. 2000). It is not yet known whether the source of this discrepancy lies in baryonic, dark-matter physics, or numerical issues in the simulations.

If the general Fall & Efstathiou view of disk formation is correct, there are several rather robust expectations that are worth exploring through the observations of high-redshift galaxies.

*The size-redshift relation.* The sizes of galactic disks forming at a redshift  $z$  should be a fixed fraction of the size of the dark-matter halo. The virial-radius of a dark-matter halo scales with redshift and virial velocity  $V_{\text{vir}}$  or virial mass  $M_{\text{vir}}$  as

$$R_{\text{vir}} = \left[ \frac{GM_{\text{vir}}}{100H^2(z)} \right]^{1/3} = \frac{V_{\text{vir}}}{10H(z)}, \quad (1)$$

where

$$H(z) = H_0[\Omega_m(1+z)^3 + \Omega_k(1+z)^2 + \Omega_\Lambda]^{1/2} \quad (2)$$

is the Hubble parameter at redshift  $z$  (Carroll et al. 1992). Assuming that the exponential scale-length  $R_s$  of the baryonic disk scales with the virial radius, the sizes of disks are expected to scale with redshift as  $R_s \propto H^{-1}(z)$  at fixed circular velocity, or  $R_s \propto H^{-2/3}(z)$  at fixed mass. Observations are more suitable to tracking evolution with fixed luminosity  $L$ , which may be expected to fall somewhere in between these two functional forms. Previous observations have demonstrated that high-redshift galaxies are small (e.g. Lowenthal et al.

<sup>1</sup> Based on observations obtained with the NASA/ESA *Hubble Space Telescope* (HST), the European Southern Observatory, and the Kitt Peak National Observatory (KPNO). HST is operated by the Association of Universities for Research in Astronomy, Inc. (AURA) under NASA contract NAS5-26555. KPNO is part of the National Optical Astronomy Observatories, which is operated also by AURA under cooperative agreement with the National Science Foundation.

<sup>2</sup> Space Telescope Science Institute, 3700 San Martin Drive, Baltimore, MD 21218, USA

<sup>3</sup> Department of Physics and Astronomy, The Johns Hopkins University, 3400 N. Charles St., Baltimore, MD 21218

<sup>4</sup> University of Melbourne, Australia

<sup>5</sup> Caltech, MS 105-24, Pasadena CA

<sup>6</sup> Laboratory for Astronomy and Solar Physics, Code 681, Goddard Space Flight Center, Greenbelt MD 20771

<sup>7</sup> Department of Astronomy and Astrophysics, University of California, Santa Cruz, CA 95064.

<sup>8</sup> University of Arizona

<sup>9</sup> Dept. of Astronomy, University of California, Berkeley Berkeley CA. 94720-3411

<sup>10</sup> Jet Propulsion Laboratory, California Institute of Technology, Mail Stop 169-506, Pasadena, CA 91109, USA

<sup>11</sup> Visiting astronomer Kitt Peak National Observatory.

1997; Bouwens et al. 2003). The larger sample of galaxies provided by GOODS allows a closer look at the trend with redshift.

*The size distribution.* If governed primarily by the angular momenta of their halos, the sizes of disk galaxies should show a log-normal distribution proportional to the dimensionless spin parameter:

$$p(\lambda)d\lambda = \frac{1}{\sqrt{2\pi}\sigma_\lambda} \exp\left[-\frac{\ln^2(\lambda/\bar{\lambda})}{2\sigma_\lambda^2}\right] \frac{d\lambda}{\lambda}, \quad (3)$$

where  $\lambda$  is related to the total angular momentum  $J$ , energy  $E$ , and mass  $M$  of the dark matter halo through the definition  $\lambda \equiv J|E|^{1/2}G^{-1}M^{-5/2}$ . The predicted functional form for the distribution of disk-galaxy sizes appears to be a reasonable match to observations of present-day disk galaxies, albeit with a width  $\sigma$  that is significantly smaller than predicted by tidal-torque theory (de Jong & Lacey 2000). It is sensible to imagine that a simple proportionality between galaxy radius and halo radius might hold even for elliptical galaxies, although models are less well developed in this case. It is less obvious that the size distribution should show the same functional form.

*The ellipticity distribution.* The theory described above is specific to disk galaxies. It is thus interesting to test whether or not high-redshift galaxies are predominantly disks. A relatively straightforward test is to compare the observed distribution of axial ratios to the distribution expected for disks or spheroids viewed at a random set of orientations, applying the classic test outlined by Sandage et al. (1970).

Throughout this paper we use a cosmology with parameters  $h, \Omega_{\text{tot}}, \Omega_m, \Omega_\Lambda = 0.7, 1.0, 0.3, 0.7$ , in the notation of Carroll et al. (1992). The sizes of galaxies quoted in this paper are in physical (proper), not co-moving, units. All magnitudes are on the AB system (Oke 1974).

## 2. OBSERVATIONS AND MEASUREMENTS

The Chandra Deep Field South (CDF-S) and Hubble Deep Field North (HDF-N) were observed with the Hubble Space Telescope (HST) Advanced Camera for Surveys (ACS) as part of the Great Observatories Origins Deep Survey (GOODS). For the HDF-N, U-band observations were carried out using the Mosaic camera on the 4-m Mayall telescope. Details of the observations, data reduction, and catalog generation are described in Giavalisco et al. (2003a). Samples of galaxies in broad bins of redshift were constructed using the Giavalisco et al. (2003b) Lyman-break selection for  $z > 3$  and the Mobasher et al. (2003) CDF-S photometric redshifts (for two bins spanning the range  $z = 1 - 1.9$  and  $z = 1.9 - 2.8$ ). The  $z \approx 3$  and 4 samples use data from both the HDF-N and the CDF-S. The  $z \approx 3$  sample is drawn only from the HDF-N, where deep U-band images exist. Because the redshift selection is based entirely on photometry, there is undoubtedly some scatter of galaxies from one redshift bin to another, and a few interlopers from lower redshifts in the high redshift bins. Based on simulations of template galaxies of various spectral types observed at the GOODS S/N, we expect the contamination to affect only the tails of the observed size, ellipticity, and concentration-index distributions. Spectroscopic confirmations are of course highly desirable.

Two different techniques were used to measure the radii of the galaxies. Half-light radii (denoted by  $r_h$ ) were measured using SExtractor (Bertin & Arnouts 1996). For this analysis SExtractor performs circular-aperture photometry using an analysis aperture radius that is ten times larger than the first radial-moment of the light distribution defined by connected pixels more than  $0.6 \sigma$  brighter than the background in a smoothed detection image. Petrosian (1976) radii were measured using the prescription adopted for the SDSS project (Stoughton et al. 2002). The ratio of the semi-minor to semi-major axis  $b/a$  is measured by SExtractor using second moments of the light distribution within the analysis aperture.

To compare the sizes of galaxies in different redshift intervals, we confine our samples to non-evolving rest-frame luminosities between  $0.7L^*$  and  $5L^*$ , where  $L^*$  is the characteristic luminosity of a  $z = 3$  Lyman break galaxy from Steidel et al. (1999). Five samples in different bins of redshift ( $z \approx 1.4, 2.3, 3.0, 4.0$ , and  $5.0$ ) are constructed. For each sample we select galaxies within the desired luminosity range based on their apparent  $z$ -band magnitudes, after accounting for cosmological effects and  $k$ -corrections assuming a typical Lyman-break galaxy spectral-energy distribution (SED). The adopted SED is from the 1999 version of the Bruzual & Charlot (1993) solar-metallicity models, with a Salpeter initial-mass function, constant star-formation rate, and age of 144 Myr. This is attenuated assuming  $E(B - V) = 0.14$  with the Calzetti et al. (2000) extinction curve to match the mean UV spectral slope seen in the  $z \sim 3$  samples (Adelberger & Steidel 2000). The luminosity range translates to a  $z$ -band magnitude range of 23.1 to 25.3 for the  $z \sim 4$  sample, with that magnitude range shifting by  $-2.41, -1.12, -0.64$ , and  $+0.46$  magnitudes for the samples in the redshift bins at  $z \sim 1.4, 2.3, 3.0$ , and  $5.0$ , respectively. After rejecting sources classified as stellar (SEXTRACTOR CLASS\_STAR > 0.9) or with unreliable photometry (SEXTRACTOR FLAG > 3), the sample sizes (for the lowest to highest redshift bins, respectively) are 21, 73, 140, 386, and 153 galaxies.

## 3. RESULTS

The galaxy sizes are measured in the band closest to rest-frame  $1500\text{\AA}$ . At  $z = 3, 4$ , and  $5$ , the central wavelengths of the F606W, F775W, and F850LP band filters fall at rest-frame  $\lambda = 1500 \pm 40 \text{\AA}$ . For the lower-redshift samples the size measurement was made in the F435W images corresponding to  $\lambda \sim 1800\text{\AA}$  at  $z = 1.4$  and  $\lambda \sim 1300\text{\AA}$  at  $z = 2.3$ . The sizes for any of these samples do not change appreciably when measured through the next redder bandpasses.

The measured size-redshift relation for our samples is shown in Fig. 1. The observed points are uncorrected for biases or incompleteness (see §4), and the errorbars represent the standard error of the mean for each sample, ignoring possible effects of clustering (Somerville et al. 2003) or crowding. The measurements are roughly consistent with constant angular sizes above  $z = 2.5$ . For comparison, in Fig. 1 we show three size-redshift relations. The blue line is the angular-size redshift relation for a standard measuring-rod in the WMAP cosmology (Spergel et al. 2003). In this cosmology, angular diameters increase by 23% from  $z = 3$  to  $z = 5$  (for objects

with fixed proper diameters). The two lines that decrease with redshift are the expected scalings if size at fixed luminosity tracks size at fixed virial velocity  $r \propto H^{-1}(z)$  or fixed mass  $r \propto H^{-2/3}(z)$ . The mean half-light radius of  $0.24''$  at  $z \approx 4$  corresponds to 1.7 kpc.

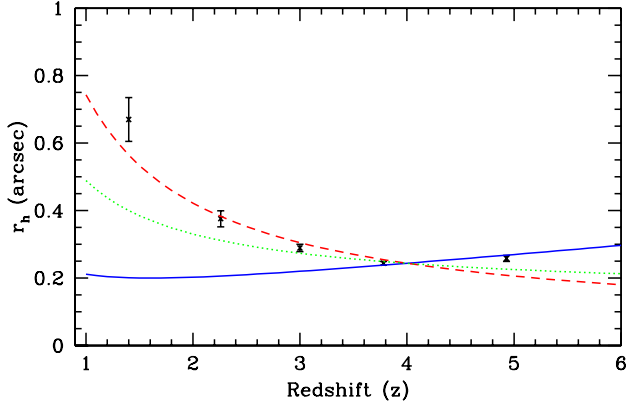


FIG. 1.— Size vs. redshift relation. Mean SExtractor half-light radii are plotted with errorbars indicating the standard error of the mean (i.e. the sample standard deviation divided by the square-root of the sample size). The solid blue curve shows the expected trend in the WMAP cosmology if physical (proper) sizes do not evolve. The dashed red curve shows the trend if sizes evolve as  $H^{-1}(z)$  and the dotted green curve shows  $H^{-2/3}(z)$ . The curves are all normalized to the mean size at  $z \approx 4$  (approximately  $r_h = 1.7$  kpc).

The size distributions of galaxies in the different redshift bins are shown in Fig. 2. The curves show a “no-evolution” model tuned to match the observed size distribution at  $z = 4$ . This model accounts for selection and measurement biases (including cosmological surface-brightness dimming) as described in §4. The galaxies in the two low-redshift bins are clearly systematically larger than the no-evolution model would predict. However, given the sample sizes and measurement biases, the trend between redshifts  $z = 3$  and  $z = 5$  is not easily distinguished from the no-evolution model.

Figure 3a compares the observed distribution of ellipticities for the B-dropout  $z \approx 4$  sample to simulations. The observed population has a larger proportion of galaxies with axial ratios  $b/a \lesssim 0.4$  than expected for a purely spheroidal population. A Kolmogorov-Smirnov test indicates a likelihood of 57% that observed distribution could have been drawn from the model disk distribution, while the probability is  $5 \times 10^{-7}$  that the observed distribution could have been drawn from the model spheroidal distribution. Similar results (at lower significance) are obtained for the  $z \sim 3$  and  $z \sim 5$  samples. However, these statistical probabilities are sensitive to the size and magnitude distribution of galaxies fed into the simulations. While we have attempted to match the observed distribution of magnitudes and sizes (and colors) at  $z = 4$  (see Fig. 2), more work is needed to verify that the preference

for flattened systems is indeed robust. Visual inspection of the images reveals very few galaxies that have morphologies reminiscent of nearby disk galaxies. The observed flattening distribution is probably a reflection of the tendency for many of the Lyman-break galaxies to have a few concentrations of light of nearly equal brightness rather than a central dominant concentration.

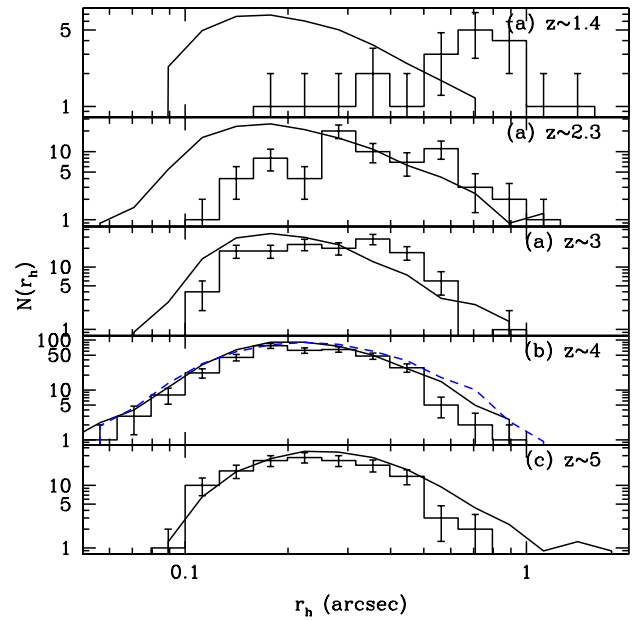


FIG. 2.— Observed size distributions. Data for the different samples are shown with Poisson error bars. The curves show a “no-evolution” model of the size distribution, tuned to match approximately the observed distribution at  $z \approx 4$ . The model has a log-normal distribution of radii with a peak at 2.1 kpc (for  $L = 2.9L^*$ ) and a width  $\sigma = 0.3$ . We adopt the size–luminosity relation ( $R \propto L^{1/3}$ ), observed for local disks (de Jong & Lacey 2000). The models include a 50/50 mix of oblate ellipticals and flat exponential disks. Model galaxies have been inserted into the images in a Monte-Carlo fashion and detected and measured using SExtractor in the same way as the real galaxies. Therefore the model curves faithfully represent the effects of both sample incompleteness and measurement biases. The input distribution (prior to selection and measurement biases) for the  $z \approx 4$  bin is shown as the dashed curve. Objects classified by SExtractor neural-network as stellar at greater than 90% probability are excluded from the samples (both the data and the simulations). In practice only a few objects with  $r_h < 0.1''$  are removed.

The concentration-index distribution for the same sample is shown in Fig. 3b. The concentration index here is defined as  $5 \log(r_{80}/r_{20})$  where  $r_{80}$  and  $r_{20}$  are radii containing 80% and 20% of the galaxy flux, respectively (Conselice 2003). The observed galaxies span a broader range than the ideal disks and spheroids that populate the simulations. The  $z \approx 4$  population tends to be more centrally concentrated than pure exponentials. Nearby spiral galaxies tend to have central concentrations of light as well, but these also tend to be red, and virtually invisible in the rest-frame ultraviolet where the current measurements are made.

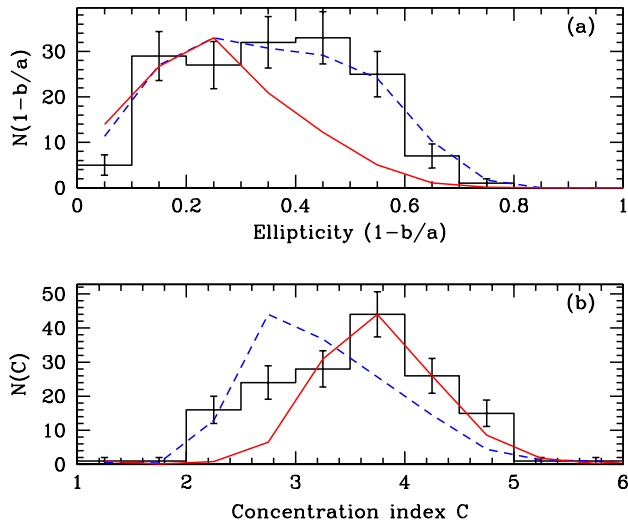


FIG. 3.— (a) Ellipticity distribution for  $z \approx 4$  galaxies compared to simulations for pure disk and pure spheroid populations (the blue-dashed and red-solid curves, respectively). For the simulations, the disk sample (viewed from arbitrary directions) is drawn from a population of oblate optically-thin spheroids with a Gaussian distribution of intrinsic axial ratios with mean  $b/a = 0.05$  and  $\sigma = 0.01$ . The spheroids are drawn from a population of oblate spheroids with intrinsic axial ratios uniformly populating the range  $0.3 < b/a < 0.9$ . The samples for both observations and simulations are limited to galaxies with  $23 < I_{775} < 25$  and SExtractor half-light radii  $r_h > 0.2''$ . (b) Concentration-index distribution for  $z \approx 4$  galaxies compared to simulations for pure disk and pure spheroid populations (the blue-dashed and red-solid curves, respectively). Samples are the same as in (a).

#### 4. SELECTION EFFECTS AND BIASES

In this section we highlight the issues of bias and incompleteness and the tests that have been carried out to verify the results of the previous sections.

*Incompleteness.* The completeness limits of the GOODS images have been estimated by inserting artificial galaxies with a wide range of half-light radii and magnitudes into the GOODS  $z$ -band image, and re-running SExtractor. The simulated galaxies have either  $r^{1/4}$ -law or exponential surface-brightness profiles, with the axial ratio distributions described in the caption to Fig. 3. The completeness limits as a function of size and magnitude are shown by Giavalisco et al. (2003a). At  $z_{850} = 24.7$ , corresponding to the mean magnitude of the  $z \approx 4$  sample considered in this letter, the sample appears to be 80% complete for galaxies with half-light radii  $r_h = 0.5''$  and 50% complete for galaxies with  $r_h = 0.9''$ . The  $z > 3$  samples are affected by incompleteness for galaxies with sizes  $r_h \gtrsim 3.5$  kpc; for the lower-redshift samples there is no equivalent bias against detecting galaxies with small sizes. Therefore the most robust result is the observation that analogs of the galaxies with small half-light radii in the  $z > 3$  bins are much less common at the lower redshifts. Without careful

modeling (or deeper images) it is not possible to rule out the possibility that galaxies with larger sizes exist at the higher redshifts. It is worth noting that a pure exponential disk galaxy with a luminosity  $L^*$  and a scale length of  $> 5$  kpc would be unlikely to be detected at  $z > 3$  in the GOODS  $z$ -band images.

*Radius-measurement biases.* The results shown in Fig. 1 and 2 are for SExtractor half-light radii. The trends and distributions look virtually identical when Petrosian radii are used. Based on the simulations it is clear that both radius measurements become biased at faint magnitudes and small sizes. For example, for galaxies in the magnitude range of our  $z \approx 4$  sample, a galaxy with an intrinsic  $r_h = 0.5''$  would have a measured  $r_h = 0.36''$ . Measurement biases will thus pull in the tail of the size distribution; the true size distributions at  $z > 3$  are almost certainly broader and peaked at slightly larger sizes than the observed distributions shown in Fig. 2. The model distribution for the  $z \sim 4$  sample provides an estimate of the importance of this bias. The true distribution of half-light radii input to the simulation is shown as the dashed line. For this input distribution the effect of selection and the size-measurement bias are minor. A distribution with a more significant tail to large sizes would show more of an effect. We have tried broader distributions and distributions with a larger mean size and found them to predict more large galaxies than observed in the  $z \approx 4$  sample.

#### 5. SUMMARY AND CONCLUSIONS

Samples of galaxies within a fixed and fairly narrow range of rest-frame UV luminosities have been compared from redshifts  $z \sim 1$  to  $z \sim 5$ . The sizes of high-redshift galaxies appear to evolve roughly as  $H^{-1}(z)$  in agreement with the rather robust expectation from hierarchical theory. This general conclusion is subject to the caveat that we may be seeing different kinds of galaxies at the different redshifts. Our sample selection necessarily targets UV-bright objects; further studies on samples selected in the near-infrared or in subsets of morphology are clearly warranted. For the galaxy sample discussed here, the size distribution at  $z \sim 4$  is reasonably well represented by a log-normal distribution, but with a smaller mean size than observed for samples of nearby luminous galaxies. Measurements of the ellipticity and concentration-index distributions suggest that Lyman-break galaxies at  $z \sim 4$  represent a mix of morphologies, with some tendency toward flattened systems.

Support for this work was provided by NASA through grant GO09583.01-96A from the Space Telescope Science Institute, which is operated by the Association of Universities for Research in Astronomy, under NASA contract NAS5-26555. Support for this work, part of the *Space Infrared Telescope Facility (SIRTF)* Legacy Science Program, was provided by NASA through Contract Number 1224666 issued by the Jet Propulsion Laboratory, California Institute of Technology under NASA contract 1407. PM acknowledges support by NASA through grant NAG5-11513.

#### REFERENCES

- Bouwens, R. J., Broadhurst, T., & Illingworth, G. 2003, astro-ph/0304547
- Bruzual, A. G., & Charlot, S. 1993, ApJ, 405, 538
- Calzetti, D., Armus, L., Bohlin, R. C., Kinney, A. L., Koornneef, J., & Storchi-Bergmann, T. 2000, ApJ, 533, 682
- Carroll, S. M., Press, W. H., & Turner, E. L. 1992, ARA&A, 30, 499
- Cole, S., Aragon-Salamanca, A., Frenk, C. S., Navarro, J. F., & Zepf, S. E. 1994, MNRAS, 271, 781
- Conselice, C. 2003, astro-ph/0303065
- Dalcanton, J. J., Spergel, D. N., & Summers, F. J. 1997, ApJ, 482, 659
- de Jong, R. S., & Lacey, C. 2000, ApJ, 545, 781
- Eke, V., Efstathiou, G., & Wright, L. 2000, MNRAS, 315, L18
- Fall, S. M., & Efstathiou, G. 1980, MNRAS, 193, 189
- Giavalisco, M., et al. 2003a, this ApJL issue
- Giavalisco, M., et al. 2003b, this ApJL issue
- Kauffmann, G., White, S. D. M., & Guiderdoni, B. 1993, MNRAS, 264, 201
- Lowenthal, J. D., et al. 1997, ApJ, 481, 673
- Mo, H. J., Mao, S., & White, S. D. M. 1998, MNRAS, 295, 319
- Mobasher, B., et al. 2003, this ApJL issue
- Navarro, J. F., & Steinmetz, M. 1997, ApJ, 478, 13
- Oke, J. B. 1974, ApJS, 27, 21
- Petrosian, V. 1976, ApJ, 209, L1
- Sandage, A., Freeman, K. C., & Stokes, N. R. 1970, ApJ, 160, 831
- Somerville, R. S., et al. 2003, this ApJL issue
- Somerville, R. S., & Primack, J. R. 1999, MNRAS, 310, 1087
- Spergel, D., et al. 2003, astro-ph/0302209
- Steidel, C. C., Adelberger, K. L., Giavalisco, M., Dickinson, M., & Pettini, M. 1999, ApJ, 519, 1
- Stoughton, C., et al. 2002, AJ, 123, 485
- White, S. D. M., & Frenk, C. S. 1991, ApJ, 379, 52
- White, S. D. M., & Rees, M. J. 1978, MNRAS, 183, 341